

Search for Higgs Bosons Decay $H \rightarrow \gamma\gamma$ Using Vector Boson Fusion

Kyle Cranmer, Bruce Mellado,
William Quayle, Sau Lan Wu

*Physics Department
University of Wisconsin - Madison
Madison, Wisconsin 53706 USA*

Abstract

The sensitivity of the ATLAS experiment to low mass SM Higgs produced via Vector Boson Fusion mechanism with $H \rightarrow \gamma\gamma$ is investigated. A cut based event selection has been chosen to optimize the expected signal significance with this decay mode. A signal significance of 2.2σ may be achieved for $M_H = 130\text{ GeV}$ with 30 fb^{-1} of accumulated luminosity.

1 Introduction

In the Standard Model (SM), there are 4 gauge vector bosons (gluon, photon, W and Z) and 12 fermions (six quarks and six leptons) [1]. These particles have been observed experimentally. The SM predicts the existence of one scalar boson, the Higgs boson [5]. The discovery of the Higgs boson remains one of the major cornerstones of the SM.

The observation of the Higgs boson is a primary focus of the of ATLAS detector [11]. It is most interesting to investigate the observability of the Higgs boson in the conditions of the LHC with the ATLAS detector.

The Higgs at the LHC is produced predominantly via gluon-gluon fusion. For Higgs masses, M_H , such that $M_H > 100$ GeV, the second dominant process is vector boson fusion (VBF). The lowest order Feynman diagram of the production of Higgs via VBF is depicted in Figure 1.

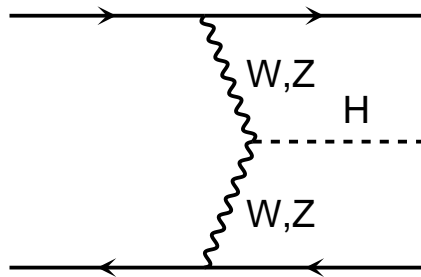


Figure 1: Lowest order Feynman diagram of the production of Higgs via VBF. The parallel solid lines correspond to quark lines.

Early analyses performed at the parton level with the decays $H \rightarrow W^+W^-$ and $H \rightarrow \tau^+\tau^-$ via VBF indicated that this mechanism could produce the most powerful discovery mode in the range of the Higgs mass, M_H , $115 < M_H < 200$ GeV [12]. The ATLAS collaboration has performed feasibility studies for these decay modes including more detailed detector description and the implementation of initial state and final state parton showers (IFSR), hadronization and multiple interactions [15]. Our group has contributed to this effort [16].

In this note we consider the production of Higgs via VBF with $H \rightarrow \gamma\gamma$. An early analysis performed at the parton level indicated that this process could be competitive with the inclusive search [18]. Another analysis performed within the ATLAS Collaboration is available [19].

The present feasibility study is addressed at low LHC luminosity (10^{33} cm $^{-2}$ s $^{-1}$) and the discovery potential is evaluated for an integrated luminosity of 30 fb $^{-1}$, which is expected to be accumulated during the first years of LHC operation.

2 MC Generation

In this Section details on the generation of signal and background processes relevant to this analysis are given.

2.1 Generation of Signal

The cross-section for the VBF process has been obtained with the matrix element calculation provided within PYTHIA6.1 [22]. The Higgs production cross-sections with the VBF mechanism as a function of M_H are given in Table 1. The Higgs branching ratio to two γ 's has been calculated with the package HDECAY [24]. Table 2 shows the values of the Higgs branching ratio to two γ 's as obtained by PYTHIA6.1 and HDECAY programs. The values obtained with PYTHIA6.1 tend to be larger than those obtained with HDECAY. In the analysis we use the the branching ratio calculated with HDECAY.

| M_H (GeV) | VBF | g-g Fusion |
|-------------|------|------------|
| 110 | 4.65 | 22.12 |
| 120 | 4.29 | 17.79 |
| 130 | 3.97 | 16.17 |
| 140 | 3.69 | 14.11 |
| 150 | 3.45 | 12.50 |
| 160 | 3.19 | 11.03 |

Table 1: Values of the Higgs production cross-section (in pb) with VBF and gluon-gluon fusion mechanisms PYTHIA6.1 for different values of M_H .

| M_H (GeV) | PYTHIA6.1 | HDECAY |
|-------------|-----------------------|-----------------------|
| 110 | $1.868 \cdot 10^{-3}$ | $1.902 \cdot 10^{-3}$ |
| 120 | $2.188 \cdot 10^{-3}$ | $2.186 \cdot 10^{-3}$ |
| 130 | $2.297 \cdot 10^{-3}$ | $2.224 \cdot 10^{-3}$ |
| 140 | $2.080 \cdot 10^{-3}$ | $1.934 \cdot 10^{-3}$ |
| 150 | $1.543 \cdot 10^{-3}$ | $1.381 \cdot 10^{-3}$ |
| 160 | $0.626 \cdot 10^{-3}$ | $0.537 \cdot 10^{-3}$ |

Table 2: Values of the Higgs branching ratio to two γ 's as obtained by PYTHIA6.1 and HDECAY for different values of M_H .

A sizable contribution from the production of Higgs via gluon-gluon fusion is expected to appear. This note is concerned with the feasibility of the observation of a Higgs signal with a dedicated event selection meant to enhance the VBF signal. Therefore, the contribution from Higgs production via gluon-gluon fusion is considered as a

signal processes. The production of this process has been modeled with PYTHIA6.1. The Higgs production cross-sections with the gluon-gluon fusion mechanism as a function of M_H are given in Table 1.

2.2 Generation of Background Processes

The relevant background processes are subdivided into two major groups. Firstly, the production of two γ 's associated with two jets. This will be called thereafter real photon production. Secondly, a sizable contribution is expected from events in which at least one jet is misidentified as a photon. This background will be referred to as fake photon production. Despite the impressive jet rejection rate after the application of γ selection criteria expected to be achieved by the ATLAS detector [11] ($\gtrsim 10^3$ for each jet) the contribution from fake photons will not be negligible due to the large cross-sections of QCD processes at the LHC.

For the inclusion of hadronization, partonic showers and multiple interaction effects the package PYTHIA6.2 is used. The factorization and renormalization scales are set to be equal. In the case of $\gamma\gamma Nj$, γNj and Nj matrix elements (ME) for $N > 0$ the scales are set to the transverse momentum, P_T , of the lowest P_T parton. This choice of the scale will yield a rather conservative estimation of the cross-section specially for γNj and Nj processes. For the case of $\gamma\gamma$ ME the scales are set to the invariant mass of the γ 's.

2.2.1 Real Photon Production

Several MC samples have been generated based on the $\gamma\gamma jj$, $\gamma\gamma j$ and $\gamma\gamma$ matrix element calculations. The $\gamma\gamma jj$ (QCD and EW ¹) and $\gamma\gamma j$ ME based MC have been obtained from MadGraphII [25] ². The $\gamma\gamma$ ME based generator in PYTHIA6.1 has been used. The latter contains the contribution from gluon-gluon fusion via a quark loop, which is not available within MadGraphII.

The following cuts have been applied at the generator level:

- Minimum transverse momentum of the jets and photons is set to 20 GeV.
- Pseudorapidity ³ of the photons, η_γ , $|\eta_\gamma| < 3$.
- Pseudorapidity of the jets, η_j , $|\eta_j| < 5$.

¹Diagrams with $\gamma\gamma jj$ in the final state display four vertexes. A diagram is called QCD if at least a gluon appears in two of the vertexes. In EW diagrams no gluon appears in any of the vertexes.

²In MadGraphII QCD and EW diagrams may be easily separated. EW $\gamma\gamma jj$ diagrams are selected by setting the maximum QCD order to 0. The QCD $\gamma\gamma jj$ ME code is obtained by setting the maximum QCD and QED orders to 2.

³Pseudorapidity, η , is defined as $\eta = -\log(\tan \theta/2)$.

- Distance in R ⁴ between jets, ΔR_{jj} , $\Delta R_{jj} > 0.7$.
- Distance in R between jets and the γ 's, $\Delta R_{j\gamma}$, $\Delta R_{j\gamma} > 0.3$.
- Distance in R between the γ 's, $\Delta R_{\gamma\gamma}$, $\Delta R_{\gamma\gamma} > 0.1$.
- Invariant mass of the γ pair, $M_{\gamma\gamma}$, $80 < M_{\gamma\gamma} < 170$ GeV.

In order to increase the efficiency of the generation of the QCD and EW $\gamma\gamma jj$ ME MC samples used for analysis in Sections 3 and 6, a cut on the difference in pseudorapidity between jets, $\Delta\eta_{jj}$, is applied such that $\Delta\eta_{jj} > 3$. The samples of QCD and EW $\gamma\gamma jj$ events have been generated in intervals of $M_{\gamma\gamma}$. The cross-sections obtained with QCD and EW $\gamma\gamma jj$ ME based MC are given in Table 3. A sample of QCD $\gamma\gamma jj$ ME MC used to perform studies reported in Section 4 has been generated without this additional cut on $\Delta\eta_{jj}$.

| $M_{\gamma\gamma}$ Range (GeV) | QCD $\gamma\gamma jj$ | EW $\gamma\gamma jj$ |
|--------------------------------|-----------------------|----------------------|
| $80 < M_{\gamma\gamma} < 110$ | 1419 | 29.79 |
| $110 < M_{\gamma\gamma} < 130$ | 581.4 | 16.14 |
| $130 < M_{\gamma\gamma} < 170$ | 709.7 | 22.16 |
| $80 < M_{\gamma\gamma} < 170$ | 2710 | 68.09 |

Table 3: Cross-sections of QCD and EW $\gamma\gamma jj$ (in fb) for different ranges of $M_{\gamma\gamma}$ as calculated by MadGraphII. A cut on $\Delta\eta_{jj} > 3$ has been applied on top of the cuts imposed at the generator level (see text).

The contribution from double parton scattering (DPS), with pairs of jets and photons coming from two independent parton collisions is not considered in the final analysis. This process contributed to some 10 – 15 % of the total background in [18]. In addition to the background processes studied in [18] we consider the production of fake photons. This background is a significant one (see Section 7). Hence the relative contribution to the total background from DPS will be about 5 – 7 %.

2.2.2 Fake Photon Production

The rate of fake photon production has been estimated by generating samples with γjjj and $jjjj$ ME based MC's. For this purpose MadGraphII is implemented.

This type of cross-section calculation involves thousands of diagrams. Generally speaking, it is convenient to separate EW and QCD diagrams. This speeds up the cross-

⁴ ΔR is defined as $\sqrt{(\Delta\phi)^2 + (\Delta\eta)^2}$.

section calculation ⁵. Unlike in the case of the $\gamma\gamma jj$ process, the EW γjjj diagrams are expected to contribute little. After the application of the cuts at the generator level used in the previous Section ⁶ (except for the cut on the invariant mass of the $\gamma\gamma$ pair) the QCD and EW γjjj diagrams yield 17.8 nb and 4.93 pb, respectively ⁷. Further cuts have been applied at the generator level:

- Maximum invariant mass between the γ and the jets (or between the jets in the case of $jjjj$ ME) should be at least 100 GeV.
- The maximum difference in pseudorapidity between jets is required to be at least 3.5 units.

After the application of these additional cuts the QCD and EW γjjj diagrams produce 6.32 nb and 1.21 pb, respectively. Assuming an effective jet rejection of the order of 10^3 , the starting cross-section for the EW γjjj process would be $\approx 1\text{ fb}$. This small cross-section will be severely reduced after the application of further selection cuts (see Section 6). In the physics analysis EW γjjj diagrams will be neglected. From now on the γjjj ME MC will include QCD diagrams only.

The situation with the $jjjj$ process is similar. Only QCD $jjjj$ diagrams will be considered in the analysis. After the application of the cuts at the generator used in the previous section a cross-section of 24650 nb is obtained. The enhancement of the $jjjj$ cross-section over that of the γjjj is striking, being at least two orders of magnitude greater than the ratio of QCD to QED coupling constants. The main contributors to the cross-sections are the subprocesses with at least one gluon in the initial state and at least two gluons in the final state. Apart from the appearance of purely gluonic diagrams ⁸ a number of diagrams in subprocesses with a quark in the initial and final state, $qg \rightarrow qggg$, appear such that the gluons in the final state come from gluon splitting.

In order to pin down severe divergence effects the cross-section from the purely gluonic subprocesses $gg \rightarrow gggg$ and $gg \rightarrow ggg$ are compared at a fixed scale (the mass of the Z boson). The cross-section for $gg \rightarrow ggg$ is ≈ 6 times larger than that of the $gg \rightarrow gggg$ subprocess. This is consistent with moderate divergence effects.

Despite the large cross-section for the $jjjj$ ME the contribution of this process to the VBF analysis is not expected to overwhelm the total background contribution.

⁵In MadGraphII the script “survey” is called before event generation. The latter performs a quick integration over the phase space with various levels of optimization. These are meant to speed up the ultimate event generation. However, in the presence of electro-weak bosons in internal lines more advanced levels of optimization may result into numerical instabilities. Therefore, the generation of EW processes is rather time consuming, specially when it comes to $2 \rightarrow 4$ processes, as in this particular case.

⁶Generator cuts specified in the bullets.

⁷In QCD γjjj diagrams the dominant subprocesses contain at least one gluon in the initial state. These type of subprocesses are suppressed in the EW γjjj diagrams

⁸As a matter of fact, the subprocess $gg \rightarrow gggg$ takes up 45% of the cross-section.

The transverse momentum distribution of the lowest P_T jets (the jets that are most likely to turn into a fake photon) with this process falls extremely rapidly. Harder cuts on the P_T of the jets and photons in the VBF analysis will significantly reduce the contribution from this background (see Section 7).

The estimation of the fake photon background based on γj and jj ME MC is not used here for the final results (see Section 7). In this case one or two tagging jets would come from the parton shower. Detailed studies performed on the production of the Z boson associated with two well separated jets have shown that the rate and the angular correlations between the tagging jets and the decay products of the boson are not described well when at least one tagging jet is produced by the parton shower [28]. The deviation from the full ME description goes beyond leading order (LO) uncertainties and it is strongly dependent on the scale set to the IFSR parton showers. It may be anticipated that the rate of fake $\gamma\gamma$ associated with two well separated jets obtained with the γj and jj ME based MC will severely underestimate a more reliable rate obtained with the γjjj ME based MC.

In order to test these assumptions a sample of γj ME based MC is produced with PYTHIA6.2. The rates of $\gamma\gamma$ associated with two well separated jets will be given in Section 6 and compared to those obtained on the basis of the γjjj ME.

3 Parton Level Analysis

As a first step, a parton level analysis is performed without the inclusion of parton shower, hadronization and multiple interaction effects. This will allow a direct comparison with the parton level analysis performed in [18]. In the latter work an earlier version of MadGraph was used to generate the signal and background MC samples. There one signal process was considered and the fake photon background was not considered.

The following event selection adopted in [18] is used here:

- a. Minimum transverse momentum of the γ 's, $P_{T\gamma 1} > 50$ GeV and $P_{T\gamma 2} > 25$ GeV. Here $P_{T\gamma 1}$ and $P_{T\gamma 2}$ correspond to the P_T of the first highest and second highest transverse momentum γ 's, respectively. The γ 's are required to fall in the central region of the detector ($|\eta| < 2.5$).
- b. The presence of two tagging jets ⁹ in opposite hemispheres is required. The tagging jets are required to lie within the acceptance of the detector ($|\eta| < 5$). The P_T of the leading jet, P_{T1} , should be $P_{T1} > 40$ GeV. The P_T of the second highest P_T jet, P_{T2} , is required to be $P_{T2} > 20$ GeV. The tagging jets should be well separated, with $\Delta\eta_{jj} > 4.4$.

⁹Tagging jet candidates are defined as the two highest P_T jets in the event.

- c. The γ 's should be in pseudorapidity in between the tagging jets with a buffer of 0.7 units.
- d. No explicit requirement on the invariant mass of the tagging jets is applied.
- e. No central jet veto survival probability correction is applied ¹⁰.
- f. The invariant mass of the γ 's should be $M_H - 1 < M_{\gamma\gamma} < M_H + 1$ GeV.

The experimental photon finding efficiency was chosen to be 80 %. The efficiency of matching a parton to a jet was set to 86 % independent on the pseudorapidity. Thus, the combined detector efficiency associated to each event is 0.473. The photon finding efficiency correction is applied after cut **a**. The parton-jet matching efficiency has been applied here after cut **b**.

| | a | b | c | f | [18] |
|-----------------------|----------|----------|----------|----------|------|
| VBF | 3.70 | 1.00 | 0.87 | 0.54 | 0.63 |
| QCD $\gamma\gamma jj$ | 169.08 | 17.55 | 5.11 | 0.52 | 0.41 |
| EW $\gamma\gamma jj$ | 5.23 | 1.93 | 1.53 | 0.15 | 0.16 |

Table 4: Effective cross-sections at parton level after successive cuts (see text). Cross-sections are given in fb for VBF signal ($M_H = 120$ GeV) and the real photon background, QCD and EW $\gamma\gamma jj$. The last column corresponds to the results quoted in Rainwater's thesis (see text).

The final state particle four-momenta are passed through the ATLFAST [30] package. This includes the smearing of the energy/momentum and position reconstructions. The parameters of the smearing applied in [18] are somewhat different. Additionally, here we use the proton structure function CTEQ5L where in [18] CTEQ4L was used instead.

The effective cross-sections after successive cuts for VBF signal ($M_H = 120$ GeV), QCD and EW $\gamma\gamma jj$ are shown in Table 4. The results obtained in [18] after all cuts, before the application of the central jet veto survival probability are shown in the last column. The VBF signal and the QCD $\gamma\gamma jj$ effective cross-section obtained here are respectively 15% smaller and 27% larger than those obtained in [18] ¹¹.

¹⁰Cuts **d** and **e** are applied in the final event selection. These bullets are placed here in order to avoid confusion in Sections 6 and 7.

¹¹A detailed analysis of the source of these discrepancies has not been performed here. However, good agreement was found between our group's results and [8] with regards to signal, QCD and EW $\gamma\gamma jj$ production. The comparison of the contribution from fake photons is still ongoing.

4 Double Counting in Real QCD $\gamma\gamma jj$ Background

In the present note the effect of initial and final state radiation is included. Events with $\gamma\gamma$ and two additional jets may be generated with $\gamma\gamma j$ ME when the second tagging jet comes from IFSR. Alternatively, two additional jets may be generated with $\gamma\gamma$ ME when the two tagging jets are produced in the parton shower. The question arises whether the $\gamma\gamma jj$ background rate calculated with the QCD $\gamma\gamma jj$ ME MC yields a conservative enough estimation from the point of view of a LO analysis.

In order to study the interplay between the ME and IFSR based production of two partons associated with $\gamma\gamma$ several MC samples have been analyzed. The analysis is performed at the parton level. Partons in the final state are ordered according to P_T . The ME generators are interfaced with PYTHIA6.2 in order to perform IFSR. In order to obtain the four-momenta of the jet originating from IFSR a clustering procedure is performed over the partons resulting from the cascade (before any hadronization occurs).

The comparison between the ME and IFSR based production of additional partons is made in two steps. Figure 2 shows the P_T distributions of the leading jet obtained with the $\gamma\gamma$ ME (solid line) and with the $\gamma\gamma j$ ME (dashed line). Here no additional requirements are applied on $\Delta\eta_{jj}$ on top of the cuts performed at the generator level (see Section 2.2.1).

In the physics analysis the cut on P_{T1} lies between 40 and 50 GeV. For these values of P_{T1} the differential cross-section obtained with $\gamma\gamma j$ ME is well above the one obtained with $\gamma\gamma$. This remains the case for events with large rapidity gaps, $\Delta\eta_{jj} > 4$. The $\gamma\gamma$ ME and $\gamma\gamma j$ ME curves may be matched by “fudging” the latter in order to meet the condition that the total cross-section be consistent with the next-to-leading order (NLO) cross-section. The K factor resulting from the NLO correction to the non-resonant production of $\gamma\gamma$ is about a factor of two [31, 32, 33].

The upper right plot in Figure 2 displays the P_T of the second jet produced by the $\gamma\gamma j$ ME (dashed line) and the QCD $\gamma\gamma jj$ ME (dotted line). The QCD $\gamma\gamma jj$ ME curve always remains above the $\gamma\gamma j$ ME curve. This remains true for events with $\Delta\eta_{jj} > 4$, as illustrated in the lower left plot of Figure 2.

For a LO type of analysis, the estimation of the $\gamma\gamma jj$ background obtained with the QCD $\gamma\gamma jj$ ME MC ¹² yields a conservative enough estimation. The addition of contributions from the $\gamma\gamma$ and $\gamma\gamma j$ ME based MC’s will lead to straight double counting, and, therefore, it will result into an unnecessary overestimation of the $\gamma\gamma jj$ background.

It is relevant to note that the central jet veto survival probability for QCD $\gamma\gamma jj$ calculated based on the parton shower approach is significantly larger than that calculated in [18]. The lower right plot in Figure 2 shows the P_T of the third jet, P_{T3} ,

¹²In addition, of course, to the EW $\gamma\gamma jj$ ME MC.

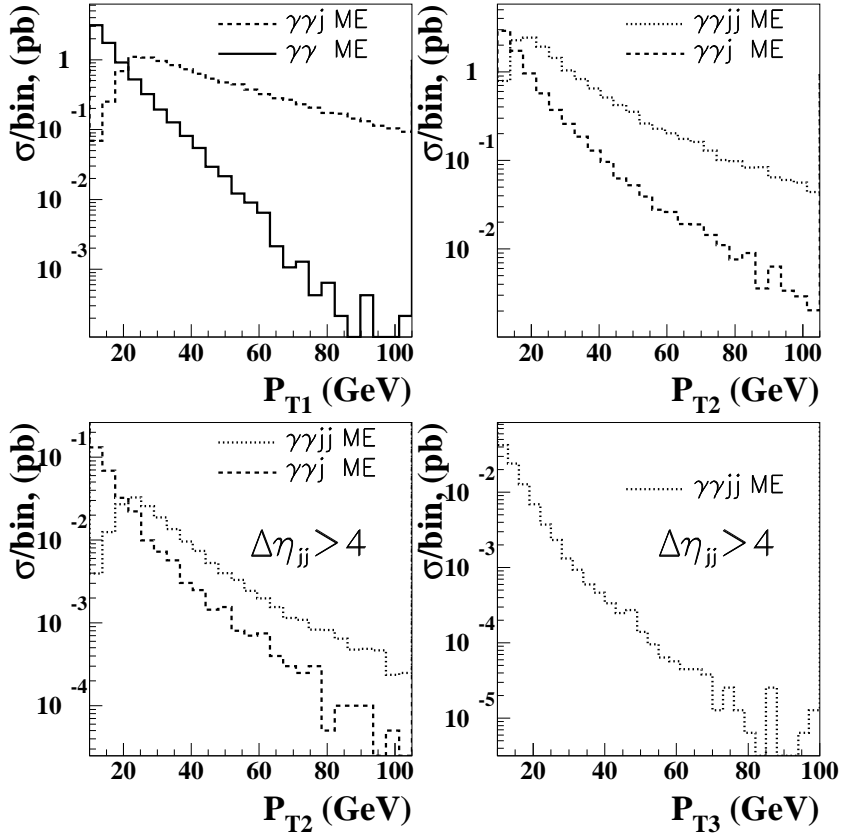


Figure 2: Transverse momentum distributions of leading jets associated with $\gamma\gamma$ production. The upper left plot displays the P_T of the leading jet produced by the $\gamma\gamma$ ME (solid line) and the $\gamma\gamma j$ ME. The upper right shows the P_T of the second jet produced by the $\gamma\gamma j$ ME (dashed line) and the QCD $\gamma\gamma jj$ ME (dotted line). The lower left plot shows similar distributions for events with $\Delta\eta_{jj} > 4$. The lower right plot corresponds to the P_T of the third jet obtained with QCD $\gamma\gamma jj$ ME for events with $\Delta\eta_{jj} > 4$.

produced by the QCD $\gamma\gamma jj$ ME MC for events with $\Delta\eta_{jj} > 4$. The probability of having an additional (non tagging) jet with $P_{T3} > 20$ GeV in the central detector region is 25% ¹³. This leads to a jet veto survival probability of the order of 75% for the QCD background, much larger than the 30% calculated in [18]. This results into an enhancement of the QCD $\gamma\gamma jj$ background with respect to the parton level based estimate obtained in [18] by a factor of ≈ 2.5 ¹⁴.

¹³This is pretty much independent on the type of hard scattering, whether we deal here with a QCD or an EW process (see Section 7 and Table 7).

¹⁴Another factor of two arises from the different size of the search mass window chosen in the physics analysis (see Section 6).

5 Detector Effects

The smearing of the energy/momentum and position reconstructions and jet clustering effects are performed with the help of the fast simulation package ATLFAST [30]. This package provides a parametrized response of the detector, based on full GEANT simulation results. The $M_{\gamma\gamma}$ resolution obtained with the help of the fast simulation is 1.2% for signal with $M_H = 120$ GeV.

The energy scale of the jets are corrected with the package ATLFASTB [30]. The parton-jet matching efficiency and the central jet fake veto obtained with ATLFAST are corrected with the help of dedicated routines [34]. The photon finding efficiency is assumed to be 80%.

The probability of a hadronic jet to be observed as a photon is available in a study presented in the ATLAS TDR [11]¹⁵. This has been parameterized as a function of the P_T of the jet. The parameterization of the central values of the fake photon probability, P_{fp} , at low luminosity yields:

$$P_{fp}(P_T) = \begin{cases} 1/p_3(P_T) & 20 < P_T < 50 \text{ GeV}; \\ 1/3400 & P_T > 50 \text{ GeV}, \end{cases}$$

where, p_3 is a third order polynomial with parameters, $a_0 = -3300, a_1 = 335.67, a_2 = -6.45, a_3 = 0.04833$. The determination of the fake photon probability is subject to systematic errors. Large errors are due to the MC statistics which was available for the initial study¹⁶. Additionally, the fake photon probability is process dependent. A study will be available in the near future, which will address these issues in more detail.

6 Optimization of the Event Selection

In this Section an event selection is obtained by means of maximizing the single bin Poisson significance for 30 fb^{-1} of accumulated luminosity and $M_H = 120$ GeV. The maximization procedure is performed with the help of the MINUIT program. A number of variables are chosen that are sensitive to the different kinematics displayed by the signal and background processes. These are common to the feasibility studies performed on most of the VBF production modes¹⁷. The following variables are chosen:

- Transverse momentum of the tagging jets.

¹⁵Volume I, page 223.

¹⁶According to the ATLAS TDR the jet rejection at low luminosity for $P_T = 20$ GeV is 1270 ± 80 , for $P_T = 40$ GeV is 2900 ± 300 . The error increases with P_T .

¹⁷For a detailed discussion see [18].

- Difference in pseudorapidity and azimuthal angle between the tagging jets, $\Delta\eta_{jj}$ and $\Delta\phi_{jj}$, respectively.
- Invariant mass of the tagging jets, M_{jj} .
- Transverse momentum of the photons.
- Difference in pseudorapidity and azimuthal angle between photons, $\Delta\eta_{\gamma\gamma}$ and $\Delta\phi_{\gamma\gamma}$, respectively.

Due to the implementation of parton shower and hadronization effects the kinematics of the final state will be somewhat different from that of the parton level analysis. In the present analysis the contribution from fake photon production has been included. As a result, the event selection needs to be re-optimized ¹⁸.

A number of pre-selection cuts are applied similar to those used to obtain the multivariate optimization in the VBF $H \rightarrow W^+W^- \rightarrow l^+l^-\not{p}_T$ analysis [36]:

- $P_{T\gamma 1}, P_{T\gamma 2} > 25 \text{ GeV}$. The γ 's are required to fall in the central region of the detector excluding the interface between the barrel and end-cap calorimeters ($1.37 < |\eta_\gamma| < 1.52$). The latter requirement reduces the acceptance by about 10%.
- Two tagging jets in opposite hemispheres ¹⁹, with $P_{T1}, P_{T2} > 20 \text{ GeV}$ and $\Delta\eta_{jj} > 3.5$.
- The γ 's should be in pseudorapidity in between the tagging jets (no buffer is required).
- Invariant mass of the tagging jets, $M_{jj} > 100 \text{ GeV}$.
- Central jet veto. No additional (non tagging) jets with $P_T > 20 \text{ GeV}$ should be observed within $|\eta| < 3.2$.
- The invariant mass of the γ 's should be $M_H - 2 < M_{\gamma\gamma} < M_H + 2 \text{ GeV}$.

The photon finding efficiency correction is applied after cut **a**. The forward jet tagging efficiency and the fake central jet veto rate corrections are applied after cuts **b** and **e**, respectively. Table 5 shows the effective cross-sections (in fb) for signal and background processes after the application of cuts **e** and **f**. The dominant background corresponds to the QCD $\gamma\gamma jj$ and the fake photon production, therefore, the optimization process will be mainly determined by the kinematics of these process together with that of the VBF signal.

¹⁸It is worth noting that here we optimize the Poissonian significance as opposed to the Gaussian approximation, S/\sqrt{B} . The optimization is also sensitive to this feature of the confidence level calculation [35].

¹⁹Tagging jets are defined as the two highest P_T jets in the event.

| Cut | VBF | g-g Fusion | QCD $\gamma\gamma jj$ | EW $\gamma\gamma jj$ | γj | γjjj | $jjjj$ |
|----------|------|------------|-----------------------|----------------------|------------|--------------|--------|
| e | 1.04 | 0.25 | 117.9 | 10.84 | 40.32 | 45. | 109.57 |
| f | 0.94 | 0.22 | 5.67 | 0.52 | 0.68 | 4.19 | 10.24 |

Table 5: Effective cross-sections (in fb) for signal and background processes after the application of cuts **e** and **f**.

The sixth column of Table 5 shows the results of fake photons obtained with the γj ME based MC. As anticipated in Section 2.2.2, the rate of fake $\gamma\gamma$ associated with two well separated jets predicted by the γj ME is expected to undershoot that obtained with the γjjj ME. Additionally, the jet and photon P_T distributions are significantly steeper in the case of the γj ME based MC. This will further suppress the contribution from this MC in the optimized event selection.

| Cut | Pre-selection | Parton Level | Optimization |
|----------|--|---|---|
| a | $P_{T\gamma 1}, P_{T\gamma 2} > 25 \text{ GeV}$ | $P_{T\gamma 1} > 50 \text{ GeV}$ $P_{T\gamma 2} > 25 \text{ GeV}$ | $P_{T\gamma 1} > 57 \text{ GeV}$ $P_{T\gamma 2} > 34 \text{ GeV}$ $\Delta\eta_{\gamma\gamma} < 1.58, \Delta\phi_{\gamma\gamma} < 3 \text{ rad}$ |
| b | $P_{T1}, P_{T2} > 20 \text{ GeV}$ $\Delta\eta_{jj} > 3.5$ | $P_{T1} > 40 \text{ GeV}$ $P_{T2} > 20 \text{ GeV}$ $\Delta\eta_{jj} > 4.4$ | $P_{T1} > 40 \text{ GeV}$ $P_{T2} > 29.5 \text{ GeV}$ $\Delta\eta_{jj} > 3.9$ |
| d | $M_{jj} > 100 \text{ GeV}$ | - | $M_{jj} > 610 \text{ GeV}$ |

Table 6: Values of the cuts applied in the pre-selection and the optimized event selection compared to those applied for the parton level analysis (see Section 3).

Figures 3-4 display the distributions of the variables chosen for the optimization of the event selection after the application of pre-selection cuts. The upper left and upper right plots in Figure 3 correspond to the transverse momentum of the leading jets. The lower left and lower right plots in Figure 3 show the difference in pseudorapidity between the leading jets and their invariant mass, respectively. The upper left and right plots in Figure 4 display the P_T of the γ 's. The lower left and right plots in Figure 4 show the difference in pseudorapidity and in azimuthal angle between the γ 's.

Initially, it has been verified that the inclusion of additional variables to those considered in [18] (see Section 3) improves the signal significance. The addition of the photon related variables, $\Delta\eta_{\gamma\gamma}$ and $\Delta\phi_{\gamma\gamma}$, improves the signal significance by some 10 – 20% depending on the Higgs mass. The implementation of those two variables separately proves more efficient than the combined $\Delta R_{\gamma\gamma}$. The inclusion of the hadronic variable $\Delta\phi_{jj}$ does not noticeably increase the signal significance. In the end the optimization is performed with 8 variables excluding $\Delta\phi_{jj}$.

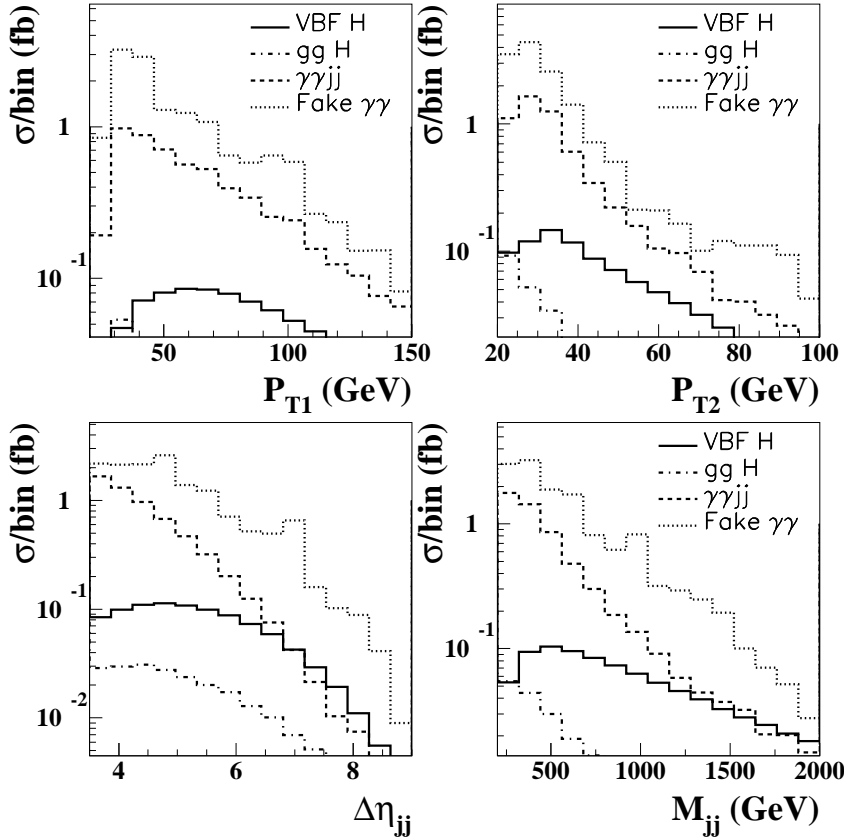


Figure 3: Kinematic distributions of signal and background processes after pre-selection cuts (see text). The upper left and upper right plots correspond to the transverse momentum of the leading jets. The lower left and lower right plots show the difference in pseudorapidity between the leading jets and their invariant mass, respectively.

Table 6 shows the results of the optimization together with the values of the cuts placed at the pre-selection level and for the parton level analysis. Due to the significant increase in the background contribution compared to the parton level analysis²⁰ the optimized event selection is significantly tighter, resulting into reduced signal and background rates (see Section 7).

²⁰The increase of the background comes from the different choice of the width of the mass window, the implementation of parton showers for the estimation of the central jet veto probability (see Section 4) and the inclusion of fake photon events.

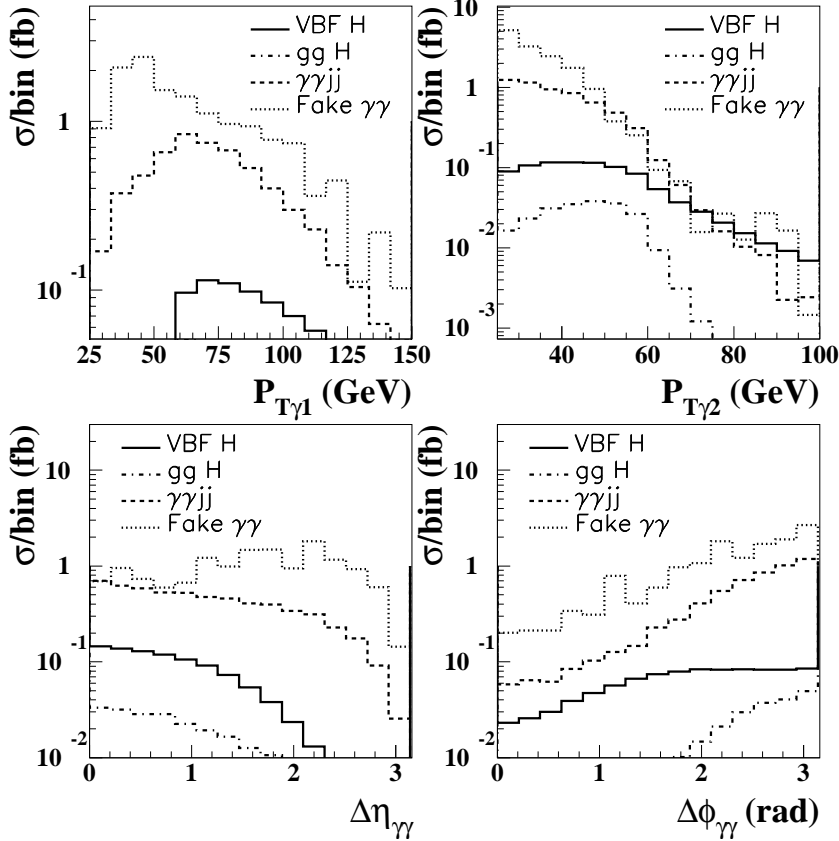


Figure 4: Kinematic distributions of signal and background processes after pre-selection cuts (see text). The upper left and right plots display the P_T of the γ 's. The lower left and right plots show the difference in pseudorapidity and in azimuthal angle between the γ 's.

7 Results and Discovery Potential

Here we use the event selection obtained in the optimization procedure performed in Section 6 (see Table 6). The expected signal and background cross-sections corrected for acceptance and efficiency corrections are shown in Table 7. Here the mass window is set for $M_H = 120$ GeV. In this table the results are given after application of successive cuts. In Table 8 results are given after the application of all cuts.

The contribution from the fake photon background has been severely reduced thanks to the inclusion of the photon angular variables (see Figure 4). The contribution from this background is, however, important. The normalization of the fake photon background is subject to sizable systematic uncertainties. This is due to the error on the determination of the fake photon rejection rate (see Section 5).

Figure 5 shows the expected signal and background effective cross-section in fb as a function of $M_{\gamma\gamma}$ for $M_H = 130 \text{ GeV}$. The dashed line shows the total background contribution whereas the dotted line corresponds to the real $\gamma\gamma$ background. The solid line displays the expected contribution of signal plus background.

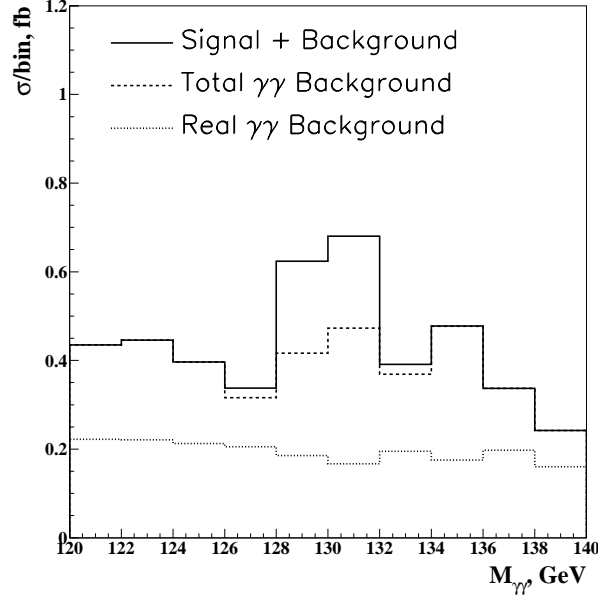


Figure 5: Expected signal and background effective cross-section in fb as a function of $M_{\gamma\gamma}$ for $M_H = 130 \text{ GeV}$. The dashed line shows the total background contribution whereas the dotted line corresponds to the real $\gamma\gamma$ background. The solid line displays the expected contribution of signal plus background.

In Table 9 results are given in terms of the total number of expected signal events, S , and background events, B , for 30 fb^{-1} of accumulated luminosity. The signal significance is given with the Gaussian approximation, S/\sqrt{B} , and the single bin Poisson calculation.

The QCD $\gamma\gamma jj$ has been estimated with QCD $\gamma\gamma jj$ ME based MC alone (see Section 4). The rate of additional (non tagging) jets has been estimated with the help of the parton shower. This approach yields a central jet veto survival probability significantly smaller than that calculated in [18]. It should not be forgotten that this feature is present in all the analyses of the VBF modes made public so far by the ATLAS collaboration. Both effects go in the direction of the overestimation of the $\gamma\gamma jj$ background. Similar discussion applies to the estimation of the fake photon background performed here.

In conclusion, the signal significance expected with this VBF mode alone reaches up to 2.2σ for 30 fb^{-1} of accumulated luminosity. These results are summarized in Figure 6. The upper and lower plots in Figure 6 display the signal significance (for 30

fb^{-1} of accumulated luminosity) and signal to background ratio dependencies on the Higgs mass.

This estimation may be improved with the implementation of a more realistic MC for the simulation of the real photon background. A better understanding of fake photon rejection would significantly help this analysis, as well.

| Cut | VBF H | g-g Fusion H | QCD $\gamma\gamma jj$ | EW $\gamma\gamma jj$ | γjjj | $jjjj$ |
|----------|-------|--------------|-----------------------|----------------------|--------------|--------|
| a | 2.25 | 5.45 | 246.90 | 7.97 | 172.60 | 691.06 |
| b | 0.73 | 0.08 | 31.83 | 4.39 | 28.30 | 35.22 |
| c | 0.70 | 0.07 | 16.81 | 4.20 | 21.76 | 30.06 |
| d | 0.57 | 0.04 | 7.43 | 3.69 | 12.77 | 16.99 |
| e | 0.42 | 0.02 | 5.41 | 2.50 | 8.52 | 8.49 |
| f | 0.38 | 0.02 | 0.28 | 0.14 | 0.22 | 0.25 |

Table 7: Expected signal and background cross-sections (in fb) corrected for acceptance and efficiency corrections after the application of successive cuts. Here $M_H = 120 \text{ GeV}$.

| M_H | VBF H | g-g Fusion H | QCD $\gamma\gamma jj$ | EW $\gamma\gamma jj$ | γjjj | $jjjj$ |
|-------|-------|--------------|-----------------------|----------------------|--------------|--------|
| 110 | 0.32 | 0.02 | 0.29 | 0.14 | 0.25 | 0.35 |
| 120 | 0.38 | 0.02 | 0.28 | 0.14 | 0.22 | 0.25 |
| 130 | 0.39 | 0.02 | 0.26 | 0.13 | 0.21 | 0.20 |
| 140 | 0.34 | 0.02 | 0.25 | 0.11 | 0.21 | 0.20 |
| 150 | 0.24 | 0.01 | 0.22 | 0.10 | 0.17 | 0.18 |
| 160 | 0.09 | 0.01 | 0.18 | 0.08 | 0.13 | 0.18 |

Table 8: Expected signal and background cross-sections, in fb , corrected for acceptance and efficiency corrections after the application of all cuts. Cross-sections are given as a function of M_H .

| M_H | S | B | S/B | S/\sqrt{B} | σ_P |
|-------|-------|-------|-------|--------------|------------|
| 110 | 10.05 | 30.69 | 0.33 | 1.82 | 1.56 |
| 120 | 12.06 | 26.54 | 0.45 | 2.34 | 2.02 |
| 130 | 12.52 | 23.97 | 0.52 | 2.56 | 2.19 |
| 140 | 10.91 | 22.90 | 0.48 | 2.28 | 1.94 |
| 150 | 7.69 | 20.15 | 0.38 | 1.71 | 1.42 |
| 160 | 2.89 | 17.21 | 0.17 | 0.70 | 0.44 |

Table 9: Expected number of signal and background events and the corresponding signal significance for 30 fb^{-1} of accumulated luminosity.

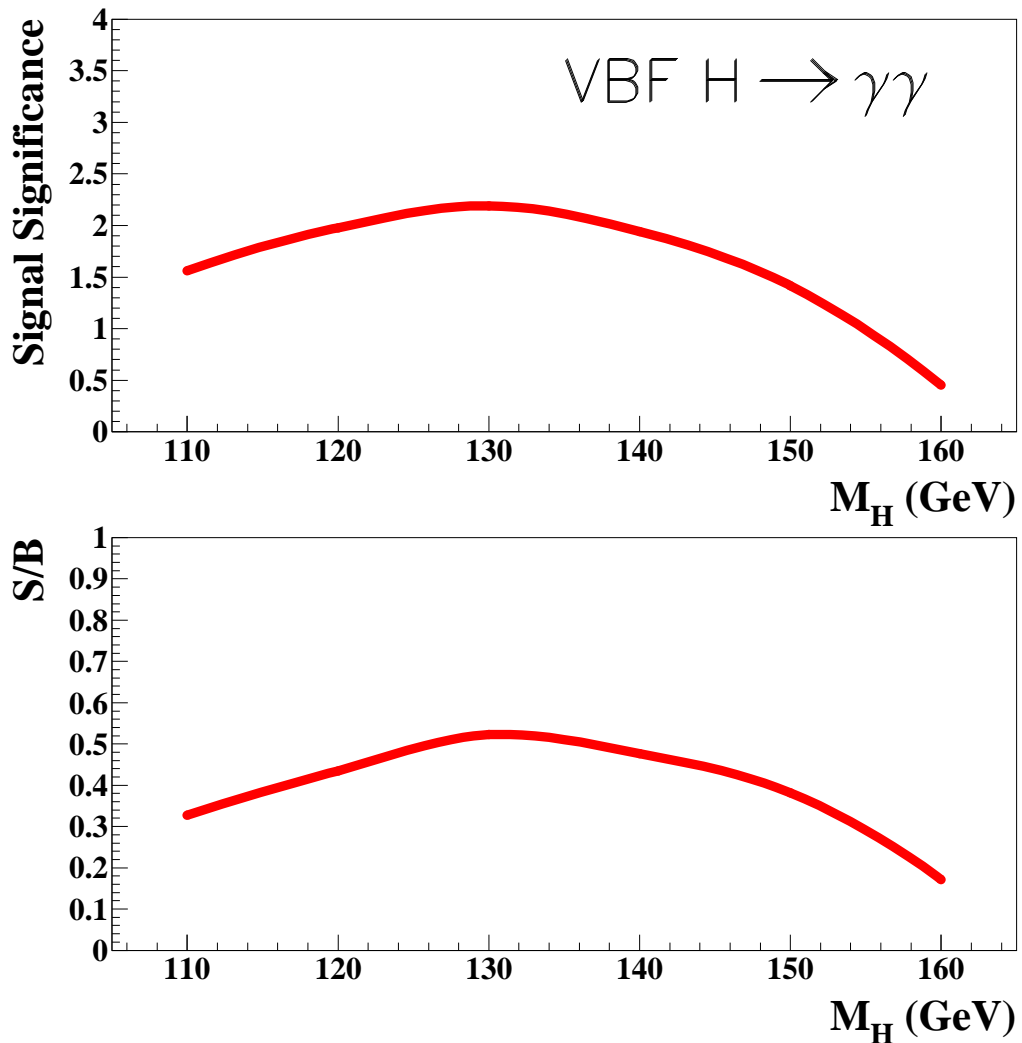


Figure 6: The upper plot displays the expected signal significance as a function of the Higgs mass for 30 fb^{-1} of accumulated luminosity. The lower plot shows the expected ratio of signal to background as a function of the Higgs mass.

References

- [1] S. L. Glashow, Nucl. Phys. **B22** (1961) 579
- [2] S. Weinberg, Phys. Rev. Lett. **19** (1967) 1264
- [3] A. Salam, Proceedings to the Eighth Nobel Symposium, May 1968, ed: N. Svartholm (Wiley, 1968) 357
- [4] S.L. Glashow, J. Iliopoulos and L. Maiani, Phys. Rev. **D2** (1970) 1285
- [5] P. W. Higgs, Phys. Lett. **12** (1964) 132
- [6] P. W. Higgs, Phys. Rev. Lett. **13** (1964) 508
- [7] P. W. Higgs, Phys. Rev. **145** (1966) 1156
- [8] F. Englert, R. Brout, Phys. Rev. Lett. **13** (1964) 321
- [9] G. S. Guralnik, C.R. Hagen and T.W.B. Kibble, Phys. Rev. Lett. **13** (1964) 585
- [10] T.W.B. Kibble, Phys. Rev. **155** (1967) 1554
- [11] ATLAS Collaboration, Detector and Physics Performance Technical Design Report, CERN-LHCC/99-14 (1999)
- [12] D. Rainwater and D. Zeppenfeld, Phys. Rev. **D60** (1999) 113004
- [13] N. Kauer *et al.*, Phys. Lett. **B503** (2001) 113
- [14] T. Plehn, D. Rainwater and D. Zeppenfeld, Phys. Rev. **D61** (2000) 093005
- [15] S. Asai *et al.*, Search for the Standard Model Higgs Boson in ATLAS using Vector Boson Fusion, ATLAS Scientific Note SN-ATLAS-2003-024 (2003)
- [16] K. Cranmer, B. Mellado, W. Quayle and Sau Lan Wu, Search for Higgs Bosons Decay $H \rightarrow W^+W^- \rightarrow l^+l^-\not{p}_T$ for $115 < M_H < 130$ GeV Using Vector Boson Fusion, ATLAS Note ATL-PHYS-2003-002 (2003)
- [17] K. Cranmer, B. Mellado, W. Quayle and Sau Lan Wu, An Update of the VBF $H \rightarrow \tau^+\tau^-$ and $\tau \rightarrow e(\mu)\nu_{e(\mu)}\nu_\tau$ Cut Analysis, ATLAS internal Communication ATL-COM-PHYS-2003-002 (2003)
- [18] D. L. Rainwater, Intermediate-Mass Higgs Searches in Weak Boson Fusion, Ph.D. thesis, University of Wisconsin - Madison, 1999
- [19] M. Minagawa, The First Result of the Study $H \rightarrow \gamma\gamma$ in VBF Process, presentation given at the ATLAS Higgs working group meeting on 04/09/02
- [20] M. Minagawa, Updated Results of the Study on $H \rightarrow \gamma\gamma$ in the VBF Process, presentation given at the ATLAS Higgs working group meeting on 12/12/02

- [21] J. Kanzaki, Study on the Background Processes for the VBF $H \rightarrow \gamma\gamma$ process, presentation given at the ATLAS Higgs working group meeting on 25/06/03
- [22] T. Sjöstrand, Comp. Phys. Comm. **82** (1994) 74
- [23] T. Sjöstrand *et al.*, Comp. Phys. Comm. **135** (2000) 238
- [24] A. Djouadi, J. Kalinowski and M. Spira, HDECAY: a Program for Higgs Boson Decays in the Standard Model and its Supersymmetric Extension, Comp. Phys. Comm. **108** (1998) 56
- [25] T. Stelzer and W. F. Long, Phys. Comm. **81** (1994) 357
- [26] F. Maltoni and T. Stelzer, MadEvent: Automatic Event Generation with MadGraph, hep-ph/0208156 (2002)
- [27] F. Maltoni and T. Stelzer, MadGraphII, <http://madgraph.physics.uiuc.edu/>
- [28] K. Cranmer, B. Mellado, W. Quayle and Sau Lan Wu, Parton Shower and Matrix Element Matching in QCD Z+2jets production, ATLAS internal Communication ATL-COM-PHYS-2003-042 (2003)
- [29] B. Mellado, Mimicking NLO MC for QCD Z+2jets and its impact on VBF $H \rightarrow \tau\tau$, presentation given at the ATLAS Higgs working group meeting on 12/12/02
- [30] E. Richter-Was, D. Froidevaux and L. Poggioli, ATLFAST2.0 a Fast Simulation Package for ATLAS, ATLAS Note ATL-PHYS-98-131 (1998)
- [31] G. Unal, HO Corrections to $\gamma\gamma j$ Background, presentation given at the ATLAS Higgs working group meeting on 12/12/02
- [32] Z. Bern, L. Dixon, C. Schmidt, Phys. Rev. **D66** (2002) 074018
- [33] T. Binoth *et al.*, Eur. Phys. J. **C16** (2000) 311
- [34] V. Cavasinni, D. Costanzo, I. Vivarelli, Forward Tagging and Jet Veto Studies for Higgs Events Produced via Vector Boson Fusion, ATLAS Note ATL-PHYS-2002-008 (2002)
- [35] K. Cranmer, B. Mellado, W. Quayle and Sau Lan Wu, Confidence Level Calculations in the Search for Higgs Bosons Decay $H \rightarrow W^+W^- \rightarrow l^+l^-\not{p}_T$ Using Vector Boson Fusion, ATLAS Note ATL-PHYS-2003-008 (2003)
- [36] K. Cranmer, B. Mellado, W. Quayle and Sau Lan Wu, Neural Network Based Search for Higgs Boson Produced via VBF with $H \rightarrow W^+W^- \rightarrow l^+l^-\not{p}_T$ for $115 < M_H < 130$ GeV, ATLAS Note ATL-PHYS-2003-007 (2003).

